REPORT

METALLURGY

Grain boundary stability governs hardening and softening in extremely fine nanograined metals

J. Hu,[1]* Y. N. Shi,[1]* X. Sauvage,[2] G. Sha,[3] K. Lu[1,3]†

Conventional metals become harder with decreasing grain sizes, following the classical Hall-Petch relationship. However, this relationship fails and softening occurs at some grain sizes in the nanometer regime for some alloys. In this study, we discovered that plastic deformation mechanism of extremely fine nanograined metals and their hardness are adjustable through tailoring grain boundary (GB) stability. The electrodeposited nanograined nickel-molybdenum (Ni–Mo) samples become softened for grain sizes below 10 nanometers because of GB-mediated processes. With GB stabilization through relaxation and Mo segregation, ultrahigh hardness is achieved in the nanograined samples with a plastic deformation mechanism dominated by generation of extended partial dislocations. Grain boundary stability provides an alternative dimension, in addition to grain size, for producing novel nanograined metals with extraordinary properties.

The strength or hardness of conventional polycrystalline metals increases with decreasing grain sizes following the classical Hall-Petch relationship (*1*, *2*); the increase in strength is reversely proportional to the square root of grain size. This relationship is established with the strengthening mechanism based on dislocation pileups at grain boundaries (GBs), which hinder dislocation motion. Plastic deformation becomes more difficult at smaller grains with higher density of GBs. Grain-size reduction into the nanometer scale makes dislocation pileup difficult, raising into question continued hardening. Experimental observations are mixed, with continuous hardening detected in some metals with grain sizes as small as 10 nm (*3*, *4*), which agrees with the experimental identification of dislocation activities in nanosized grains (*5*, *6*). Meanwhile, deviation from the Hall-Petch relation was reported for a number of nanograined samples that included cases of softening (*7*, *8*) when grain sizes were smaller than 10 to 30 nm.

The different observed behaviors for nanograined samples means that an ambiguity remains as to the governing plastic deformation mechanism in nanograined materials. Previous research attributed the observed softening to GB migration, GB sliding, or grain rotation, which are supported by experimental measurements and molecular dynamic simulations (*9*–*12*). Mechanically driven GB migration observed in various nanograined materials leads to grain coarsening and softening at ambient temperature under tension, compression, and indentation tests (*11*, *13*–*15*). Coarsening of nanograins observed in thin-film samples under plastic deformation was attributed to grain rotations (*9*). These studies regard the numerous GBs in nanograined materials not only as barriers to slip transmission, as in conventional coarse-grained materials, but also the primary facilitators for plastic deformation (*16*).

The kinetic process of the GB-mediated deformation depends on the nature of GBs. Compared with the low-energy boundaries such as twin boundary or low-angle GBs, the conventional high-angle GBs exhibit lower thermal and mechanical stability (*16*). Nevertheless, high-angle GBs can be effectively stabilized through GB relaxation (*17*), GB segregation of solute atoms (*18*, *19*), or both processes. Hence, by tailoring GB stability, we expected adjustments to the GB-mediated processes and the corresponding plastic deformation behavior. We aimed to tailor GB stability by means of GB relaxation and segregation in nanograined nickel-molybdenum (Ni–Mo) alloys with extremely fine grains in which the GB effect is greatly amplified. We present evidence that the plastic deformation and hardness of the nanograined metals are essentially governed by GB stability.

We prepared nanograined pure Ni and Ni–Mo alloy foil samples of 70 μm thickness by using DC electrodeposition, with Mo concentrations in a range of 0.8 to 21.5 atomic % (at %) (*20*). We observed with transmission electron microscopy (TEM) that the as-deposited samples consist of equiaxed nano-sized grains with random orientations. The average grain size decreases with higher Mo contents, from 30 nm in pure Ni to 3.4 nm for 21.5% Mo. In the samples, we observed extremely fine grains with a narrow size distribution without the detection of second phase (Fig. 1). This implies that the nano-sized grains are supersaturated Ni(Mo) solid solution in the high Mo-content samples because the equilibrium solid solubility of Mo in Ni is ~14%. High-resolution TEM (HRTEM) images indicated that the randomly oriented tiny grains are dislocation-free crystals (Fig. 1C). In some large grains of the pure-Ni sample, we occasionally see dislocations.

The as-deposited pure-Ni sample exhibits a microhardness of 4.34 ± 0.11 GPa, which is quantitatively consistent with the Hall-Petch plot extrapolated from the literature data (Fig. 2A) (*3*, *21*–*25*). With decreasing grain size, the microhardness increases to a maximum value of ~6.01 ± 0.04 GPa at 10 nm, then decreases to 5.02 ± 0.06 GPa at 3.4 nm (Fig. 2A). These data deviate from the extrapolated Hall-Petch line. The obvious softening is qualitatively consistent with that in electrodeposited Ni–tungsten (W) alloys with comparable grain sizes (*7*), which originates from a plastic deformation mechanism crossover from dislocation slip to a GB-mediated process at the "strongest size" (*26*), as analyzed with the post-deformation structures.

For tailoring GB stability, we annealed the as-deposited nanograined samples at modest temperatures. Annealing below 200°C for 1 hour

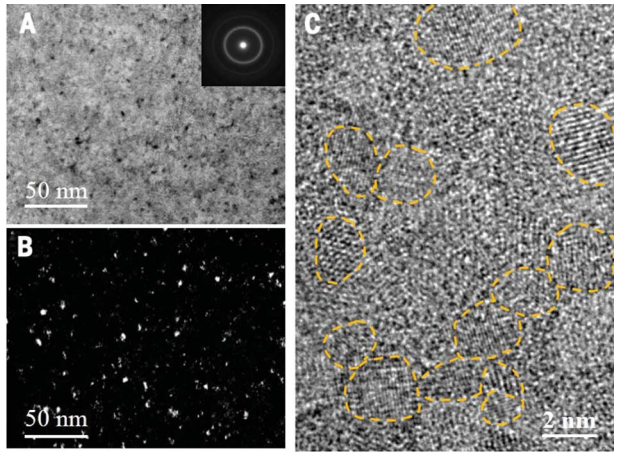

Fig. 1. Microstructure of the as-deposited nanograined Ni–Mo alloy. (**A**) Bright-field and (**B**) dark-field images of the as-deposited Ni–21.5% Mo sample. (Inset) A corresponding selected area diffraction pattern. (**C**) A HRTEM image of the same sample showing individual grains outlined by dashed lines.

[1]Shenyang National Laboratory for Materials Science, Institute of Metal Research, Chinese Academy of Sciences, Shenyang 110016, China. [2]Normandie University, UNIROUEN, Institut National des Sciences Appliquées Rouen, CNRS, Groupe de Physique des Matériaux, 76000 Rouen, France. [3]Herbert Gleiter Institute of Nanoscience, Nanjing University of Science and Technology, Nanjing 210094, China.
*These authors contributed equally to this work.
†Corresponding author. Email: lu@imr.ac.cn

induces a slight hardening in the pure nanograined Ni from 4.34 to 4.91 GPa, with little grain size change (as in Fig. 2B). The hardening is believed to originate from a GB relaxation process (*17*), with a reduced GB excess energy as verified with the differential scanning calorimetry measurements (*20*). Annealing at higher temperatures results in obvious grain-coarsening accompanied with a hardness drop, to 2.36 GPa at 400°C. Annealing-induced hardening became more pronounced in the Ni-Mo samples with higher Mo concentrations. For example, in the Ni–2.8% Mo sample, hardness increases from the as-deposited 5.88 ± 0.08 GPa to 7.51 ± 0.08 GPa when annealed at 380°C. In each Ni–Mo sample, we detected a slight increment in grain size during the peak annealing. After annealing the as-deposited sample Ni–21.5% Mo at 525°C, its hardness increased from an initial 5.02 GPa to a value of 11.35 ± 0.16 GPa, with an average grain size of 8.2 nm (Fig. 2B). In the as-annealed state, we detected no precipitation from TEM observations and electron diffraction. The peak annealing temperature corresponded to the onset of the obvious coarsening of the nanograins. The peak temperature elevates with higher Mo contents, indicating an enhanced thermal stability of nanograins with higher Mo concentrations, irrespective of smaller sizes.

In fact, annealing-induced hardening phenomena have been observed in other nanograined samples, including pure metals (*27*–*29*) and alloys (*30*, *31*). Comparing our results with those literature data, we observed a general trend that the maximum annealing-induced hardening increases with smaller grains, especially for grain sizes below 10 nm (Fig. 2C). Such a hardening process can be attributed to either or both GB stabilization through relaxation and segregation of solute atoms.

By plotting microhardness versus grain size in the annealed nanograined samples before obvious grain coarsening, we found that the data points deviate from the as-deposited ones (Fig. 2A). For each sample, annealing induced an obvious hardness increase, although grains coarsen slightly. The hardness increase becomes larger with smaller initial grain size. For sample Ni–21.5% Mo with an initial grain size of 3.4 nm, the annealing-induced hardness increase is as much as 120% (Fig. 2C). The hardness data in other nanograined Ni alloys [Ni–W (*30*) and Ni–phosphorus (P) (*31*)] fall within the large hardness variation span of our nanograined samples in this grain-size regime (Fig. 2A). This striking feature shows that hardness of a nanograined metal can be doubled without changing grain size.

The hardness of each peak-annealed Ni–Mo sample is well above the extrapolated Hall-Petch line of Ni ($D^{-1/2}$ variation; D is average grain size). Instead, we fit the data with a D^{-1} variation (Fig. 2A). Although Mo has a solution-hardening effect on our samples, the grain size dependence we observed requires an alternative plastic deformation mechanism other than dislocation pile-up.

We analyzed chemical compositions and their distributions in the Ni–Mo samples using atom probe tomography (APT). The three-dimensional reconstruction from APT detections showed that both Ni and Mo atoms distribute homogeneously in the as-deposited Ni–14.2% Mo sample (Fig. 3, A and B). We detected trace impurities (carbon, oxygen, and nitrogen) with a total content below 0.16 at % from chemical analysis, which distribute uniformly throughout the sample in terms of APT results. After the peak annealing at 500°C, however, some nanometer-scale Mo concentration fluctuations clearly appear (Fig. 3, C and D). Quantification through linear compositional measurements of the annealed state show that the amplitude of these fluctuations is ~10 at %, with a length scale in a range of 10 to 20 nm (Fig. 3E). The average Mo concentration (18.0 ± 0.1 at %) is slightly higher than the nominal concentration of the as-deposited state (14.2 at %). We attributed this to some small-composition variations in the as-deposited material at a scale much larger than typical volumes probed by means of APT. Quantitative x-ray diffraction (XRD) analysis showed that lattice parameter (a) of Ni(Mo) solid solution in the as-deposited Ni–14.2% Mo sample is 0.3596 nm. With increasing the annealing temperature to 500°C, the XRD-measured a value dropped to 0.3583 nm (Fig. 3F), corresponding to a Mo concentration of ~12 at % (*20*). This value is ~2 at % lower than that in the as-deposited alloy, verifying the depletion of Mo in the annealed Ni grain lattice. These results seem to indicate that annealing of the as-deposited Ni–Mo samples induced Mo enrichment at GBs and depletion of nano-sized Ni(Mo) grains. In addition, segregation of impurities at GBs may also be induced through thermal annealing. Although precipitates have not been detected under detailed HRTEM observations and XRD analysis, even in the peak-annealed Ni–21.5% Mo sample, early-stage precipitation or clustering at GBs could not be excluded during annealing.

To determine the plastic deformation mechanism, we characterized post-deformation microstructures of the nanograined Ni–14.2% Mo samples after microhardness tests by means of TEM observations of cross-sectional specimens beneath the indentation. Compared with the as-deposited homogeneous nanograined structures (4.9 nm average in grain size), the plastically deformed region beneath the indent becomes structurally heterogeneous with obvious grain coarsening (Fig. 4, A to D). We observed some very large grains up to 150 nm in size mixing with small ones very close to the indented surface. Deeper from the surface, we found that grain-coarsening becomes less pronounced with less heterogeneous grain sizes from our observations (Fig. 4, A to D) and statistic grain size measurements (Fig. 4E). We did not detect any stacking fault inside grains of different sizes in the deformed regions, although dislocations are occasionally observed in some grown grains. The boundaries between neighboring nanograins are also distinct.

We can attribute the deformation-induced grain-coarsening in the as-deposited samples—analogous to previous observations in various

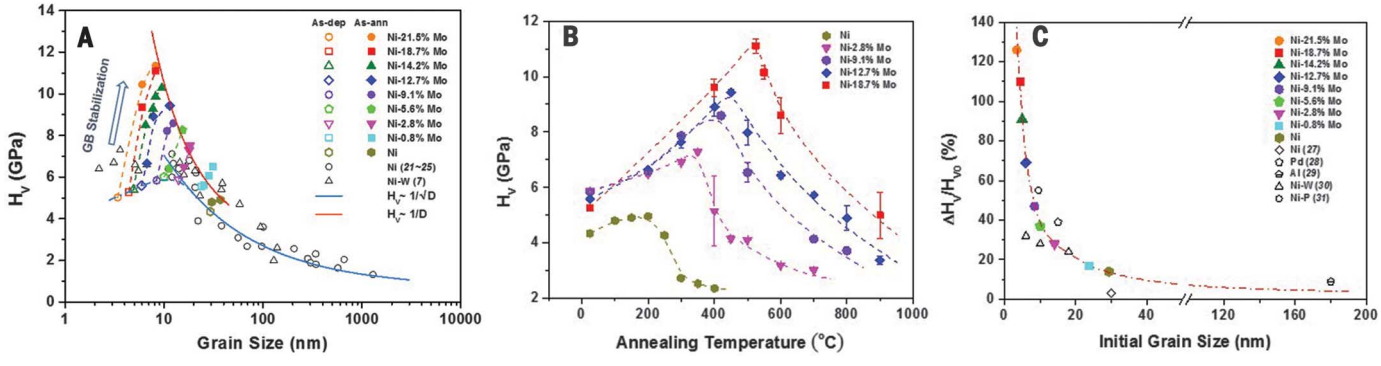

Fig. 2. Softening and hardening in the nanograined Ni–Mo alloys. (**A**) Variations of microhardness with grain size for the as-deposited (open symbols) and the as-annealed (solid symbols) Ni and Ni–Mo samples. Literature data of electrodeposited Ni and Ni–W alloys are included for comparison. The blue solid line is a Hall-Petch plot ($H_v \sim 1/\sqrt{D}$) for pure Ni extrapolated in terms of literature data. The solid red line is a fitting line by using $H_v \sim 1/D$ for the nanograined Ni and Ni–Mo samples after annealing at peak temperatures. (**B**) Microhardness variations as a function of annealing temperature (with a duration of 1 hour) for the nanograined Ni and Ni–Mo alloys with different Mo concentrations. (**C**) Variation of the maximum microhardness increment induced by annealing ($\Delta H_v/H_{v0}$; H_{v0} is the initial hardness) as a function of initial grain size for the Ni and Ni–Mo samples (solid symbols). Data reported in other nanograined materials are presented for comparison (open symbols).

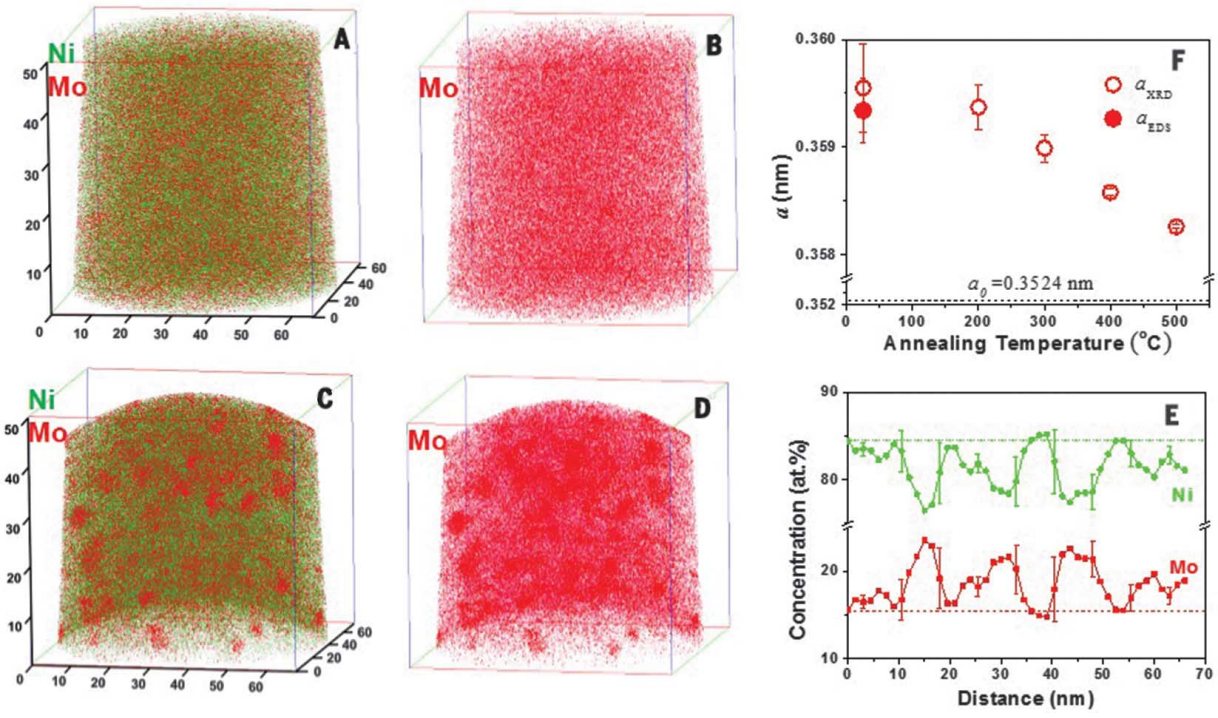

Fig. 3. Annealing-induced Mo segregation. (**A** to **D**) Three-dimensional APT reconstruction of the nanograined Ni–14.2% Mo samples.; distributions of Ni and Mo in the as-deposited state [(A) and (B)] and in the sample annealed at 500°C [(C) and (D)]. (**E**) The composition profile of Ni and Mo in the annealed sample. (**F**) Variation of lattice parameters in the sample Ni–14.2% Mo, with annealing temperature determined from quantitative XRD analysis (open circles). The calculated lattice parameter for the as-deposited sample from the energy-dispersive x-ray spectroscopy compositional analysis following Vegard's law is included for comparison (solid circle). a_0, lattice parameter of pure nickel.

nanograined samples under indentation, compression, and tension—to GB-mediated deformation processes such as mechanically driven GB migration or grain rotation (*11*, *13*–*15*). These processes may lead to the merging of nanograins associated with intergranular dislocation activities. Larger grains formed close to the indented surface are due to higher strain and stress imposed by the contact loading. The GB-mediated deformation explains the observed softening in the as-deposited samples with $D < 10$ nm as in Fig. 2A, agreeing with the molecular dynamics (MD) simulations of the deformation mechanism crossover between perfect dislocation slip and GB-mediated processes at a "strongest" grain size (*12*, *32*). The continuous softening with smaller nanograins indicated that alloying Mo up to 21.5 at % is ineffective to suppress GB-mediated plasticity of Ni nanograins under the present straining conditions.

We detected very different deformed microstructures in the as-annealed sample. The as-annealed Ni–14.2% Mo sample (annealed at 500°C) before deformation consists of homogeneous nanograins with random orientations and an average size of 9.5 nm (Fig. 4F). Compared with the as-deposited structure, we noticed some lattice defects such as stacking faults or twins only in a small fraction of grains in the annealed sample. After indentation, grains become slightly larger beneath the indented surface, with an average size of 12 nm (Fig. 4E). However, we found stripped contrasts inside most of the grains (Fig. 4G). HRTEM observations clarified the presence of multiple stacking faults and twins in the tiny grains (Fig. 4H). Orientations of the multiple stacking faults seem different from grain to grain. In each grain, the stacking faults are parallel to each other, with extremely small spacing, penetrating through the grains where we observed plenty of partial dislocations.

A negligible grain size increase after deformation indicated suppression of the mechanically driven grain coarsening, implying that GBs in the annealed sample are stable against straining. We attributed the inherent GB stability in the annealed samples to structural relaxation and Mo segregation at GBs, which substantially lower the GB energy. Measured GB excess energy in the as-deposited nanograined Ni–Mo sample decreased by ~7 to 30% after annealing at the peak temperatures (the reduction increased with higher Mo concentrations) (*20*). Reduced GB energy stabilizes the nanograined structures as the thermodynamic driving force for grain coarsening is lowered. In addition, enrichment of Mo and trace impurities at GBs provides a kinetic stabilization of the nanograins (*33*).

Segregation of Mo and other trace impurities stabilized GBs so that the dominant plastic deformation is changed from the GB-mediated process to generation of extended partial dislocations. According to the generalized planar fault energy curve from MD simulations (*34*), an increased ratio of the unstable to the stable stacking fault energy may result in the extended stacking faults by transection of leading partials through the entire grain without emission of trailing partials. Mo segregation may cause relaxation of local stress levels at GBs (and triple junctions) (*35*) and, as a result, prevent the emission of the trailing partials, enhancing the formation of extended stacking faults. This analysis agrees with our observation of a high density of stacking faults in the as-annealed nanograined Ni–Mo solid solution [with a high stacking fault energy of 90 mJ/m^2 at 12 at % Mo (*36*)], in contrast to that in other nanograined metals such as aluminum (*37*) with similar high stacking fault energies in which stacking faults and twins were found only occasionally. Copious nucleation of extended dislocations at the stabilized GBs requires a very high applied stress that is inversely proportional to grain size ($1/D$) for the nanograins (*32*). This explains the observed extremely high hardness and $1/D$ dependence in the as-annealed nanograined Ni–Mo samples.

Although the atomistic mechanism of the mechanically driven GB migration still needs clarification, we believe that GB migration is mediated by full dislocation slip and its interactions with the GB, as indicated by atomistic simulations. However, we did not notice obvious GB migration in the as-annealed state in which we detected high-density extended dislocations. This means that the extended partial dislocation slip is

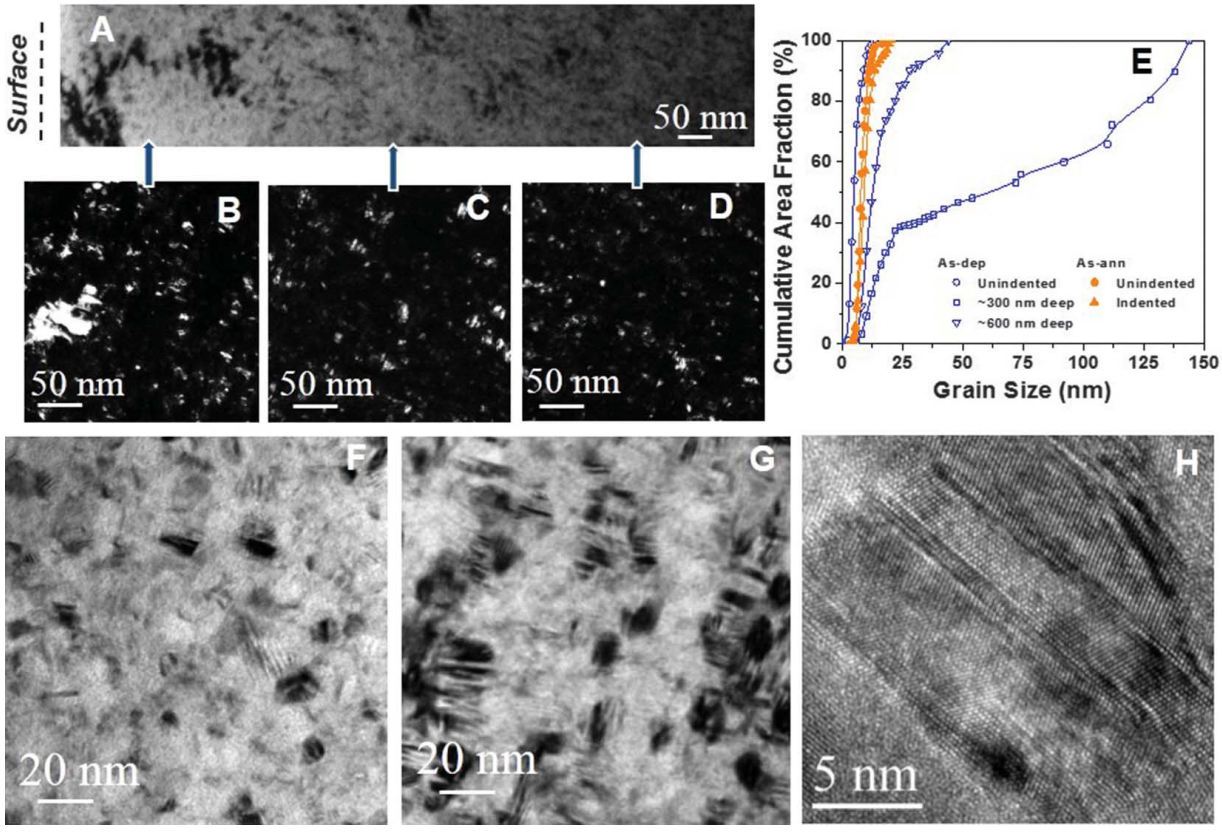

Fig. 4. Deformation mechanisms in the as-deposited and the as-annealed nanograined Ni–Mo samples. (**A**) A typical bright-field TEM image taken underneath the indented surface (indicated by dashed line) in the as-deposited Ni–14.2% Mo sample after microhardness test, with (**B** to **D**) corresponding dark-field images at different depths from the surface (indicated by arrows) (**E**) The cumulative fraction of grains area versus grain size in the subsurface layer of the as-deposited and the as-annealed Ni–14.2% Mo sample before and after microhardness test, respectively. For the as-deposited sample, two sets of data at depths of ~300 and ~600 nm from the indented surface are included. (**F** and **G**) Typical bright-field TEM images taken at <200 nm deep below the (indented) surface in the annealed Ni–14.2% Mo sample before and after microhardness test, respectively. (**H**) A HRTEM image of a grain in (G).

not effective in inducing GB migration even under much higher stress. In fact, we scarcely observed partial dislocations in the as-deposited samples with obvious grain coarsening. The plastic deformation of the as-annealed nanograined samples is clearly accommodated by extended partial dislocations alone, fundamentally distinct from that by the cooperative process of GBs and lattice dislocations in the as-deposited state with comparable grain sizes.

The present study clarifies that stability of GBs plays a crucial role in determining the plastic deformation and hardness of nanograined materials, especially with extremely fine grains. For GBs with a low stability against plastic straining, deformation mechanism shifts from full dislocation slip to GB-mediated process at a critical grain size, leading to softening. In nanograined samples with inherent GB stability in which GB-mediated processes are suppressed, plastic deformation is carried by extended partial dislocations at small sizes, resulting in substantial hardening. Hence, hardness of nanograined metals is not only grain size–dependent but governed by GB stability as well, which explains the reported controversial results on hardening and softening behaviors in nanograined materials. Stability of interfaces provides an alternative dimension for tailoring properties and performance of nanostructured materials. Novel nanostructured materials with extraordinary properties such as ultrahigh hardness could be synthesized by manipulating both characteristic size and interface stability.

REFERENCES AND NOTES

1. E. O. Hall, *Proc. Phys. Soc. London B* **64**, 747–753 (1951).
2. N. J. Petch, *J. Iron Steel Inst.* **174**, 25–28 (1953).
3. J. A. Knapp, D. M. Follstaedt, *J. Mater. Res.* **19**, 218–227 (2004).
4. J. Chen, L. Lu, K. Lu, *Scr. Mater.* **54**, 1913–1918 (2006).
5. D. A. Hughes, N. Hansen, *Phys. Rev. Lett.* **112**, 135504 (2014).
6. B. Chen *et al.*, *Science* **338**, 1448–1451 (2012).
7. A. J. Detor, C. A. Schuh, *Acta Mater.* **55**, 371–379 (2007).
8. M. A. Meyers, A. Mishra, D. J. Benson, *Prog. Mater. Sci.* **51**, 427–556 (2006).
9. Z. Shan *et al.*, *Science* **305**, 654–657 (2004).
10. L. Wang *et al.*, *Nat. Commun.* **5**, 1–7 (2014).
11. T. J. Rupert, D. S. Gianola, Y. Gan, K. J. Hemker, *Science* **326**, 1686–1690 (2009).
12. J. Schiøtz, K. W. Jacobsen, *Science* **301**, 1357–1359 (2003).
13. T. H. Fang, W. L. Li, N. R. Tao, K. Lu, *Science* **331**, 1587–1590 (2011).
14. D. Pan, S. Kuwano, T. Fujita, M. W. Chen, *Nano Lett.* **7**, 2108–2111 (2007).
15. K. Zhang, J. R. Weertman, J. A. Eastman, *Appl. Phys. Lett.* **85**, 5197–5199 (2004).
16. K. Lu, *Nat. Rev. Mater.* **1**, 16019 (2016).
17. A. Hasnaoui, H. Van Swygenhoven, P. M. Derlet, *Acta Mater.* **50**, 3927–3939 (2002).
18. J. Weissmüller, *Nanostruct. Mater.* **3**, 261–272 (1993).
19. R. Kirchheim, *Acta Mater.* **50**, 413–419 (2002).
20. Materials and methods are available as supplementary materials.
21. G. D. Hughes, S. D. Smith, C. S. Pande, H. R. Johnson, R. W. Armstrong, *Scr. Metall. Mater.* **20**, 93–97 (1986).
22. F. Dalla Torre, H. Van Swygenhoven, M. Victoria, *Acta Mater.* **50**, 3957–3970 (2002).
23. A. M. El-Sherik, U. Erb, G. Palumbo, K. T. Aust, *Scr. Metall. Mater.* **27**, 1185–1188 (1992).
24. F. Ebrahimi, G. R. Bourne, M. S. Kelly, T. E. Matthews, *Nanostruct. Mater.* **11**, 343–350 (1999).
25. C. A. Schuh, T. G. Nieh, T. Yamasaki, *Scr. Mater.* **46**, 735–740 (2002).
26. S. Yip, *Nature* **391**, 532–533 (1998).
27. Y. M. Wang *et al.*, *Scr. Mater.* **51**, 1023–1028 (2004).
28. J. R. Weertman, P. G. Sanders, *Diffus. Defect Data Solid State Data Pt. B Solid State Phenom.* **35-36**, 249–262 (1994).
29. X. Huang, N. Hansen, N. Tsuji, *Science* **312**, 249–251 (2006).

30. T. J. Rupert, J. R. Trelewicz, C. A. Schuh, *J. Mater. Res.* **27**, 1285–1294 (2012).
31. L. Chang, P. W. Kao, C. H. Chen, *Scr. Mater.* **56**, 713–716 (2007).
32. V. Yamakov, D. Wolf, S. R. Phillpot, A. K. Mukherjee, H. Gleiter, *Nat. Mater.* **3**, 43–47 (2004).
33. C. C. Koch, R. O. Scattergood, M. Saber, H. Kotan, *J. Mater. Res.* **28**, 1785–1791 (2013).
34. H. Van Swygenhoven, P. M. Derlet, A. G. Frøseth, *Nat. Mater.* **3**, 399–403 (2004).
35. V. Yamakov, D. Wolf, S. R. Phillpot, A. K. Mukherjee, H. Gleiter, *Philos. Mag. Lett.* **83**, 385–393 (2003).
36. T. C. Tiearney, N. J. Grant, *Metall. Trans. A Phys. Metall. Mater. Sci.* **13**, 1827–1836 (1982).
37. M. Chen *et al*., *Science* **300**, 1275–1277 (2003).

ACKNOWLEDGMENTS

The authors appreciate financial support from the Ministry of Science and Technology of China (grant 2012CB932201), the National Science Foundation of China (grants 51231006 and 51571120), and the Chinese Academy of Sciences (grant KGZD-EW-T06). The authors thank N. N. Liang at Nanjing University of Science and Technology for his kind help on APT sample preparation. Data of sample characterization including grain size, lattice parameter, chemical compositions, microhardness, and GB energy are available in the supplementary materials.

SUPPLEMENTARY MATERIALS

www.sciencemag.org/content/355/6331/1292/suppl/DC1
Materials and Methods
Fig. S1
Table S1

1 December 2016; accepted 14 February 2017
10.1126/science.aal5166

Grain boundary stability governs hardening and softening in extremely fine nanograined metals

J. Hu, Y. N. Shi, X. Sauvage, G. Sha and K. Lu (March 23, 2017)
Science **355** (6331), 1292-1296. [doi: 10.1126/science.aal5166]

Editor's Summary

Nanograined metals avoid going soft

The Hall-Petch relationship links a metal's increasing hardness with decreasing grain size, but it breaks down when grains become very small. This is unfortunate because nanograined metals could otherwise be extremely hard. Hu *et al.* found a way to circumvent this problem in a set of nickel-molybdenum alloys. They altered the molybdenum composition and annealed the samples at just the right temperature, which stabilized the grain boundaries in their nanograined samples. This allowed hardness to keep increasing with decreasing grain size, which could provide a route for designing superhard coatings.

Science, this issue p. 1292